

Search for Lorentz violation in short-range gravity

J.C. Long and V. Alan Kostelecký

Physics Department, Indiana University, Bloomington, IN 47405, U.S.A.

(Dated: IUHET 589, December 2014)

Abstract

A search for sidereal variations in the force between two planar tungsten oscillators separated by about $80\ \mu\text{m}$ sets the first experimental limits on Lorentz violation involving quadratic couplings of the Riemann curvature, consistent with no effect at the level of $10^{-9}\ \text{m}^2$.

arXiv:1412.8362v1 [hep-ex] 29 Dec 2014

Local Lorentz invariance is a foundational component of General Relativity (GR), which currently remains our most successful theory of gravity. However, GR is formulated as a classical theory, and merging it with quantum physics in a consistent manner may well demand changes in its foundational structure. Even if local Lorentz invariance is exact in the underlying theory of quantum gravity, spontaneous breaking of this symmetry may occur, leading to tiny observable effects [1]. Experimental studies of Lorentz invariance are therefore valuable as probes of the foundations of GR.

Short-range experiments are uniquely sensitive probes of gravity at scales below about a millimeter and hence offer interesting opportunities to search for new physics beyond GR [2]. The essence of short-range experiments is to measure the force between two masses separated by a small distance. To attain sensitivity at short range without being overwhelmed by Newton forces at larger scales, the test masses are typically scaled to that range. Experiments of this type are well suited to searching for deviations from the gravitational inverse-square law.

To date, most studies of local Lorentz invariance in gravity are restricted to matter-gravity couplings [3, 4]. However, recent theoretical work shows that general quadratic curvature couplings involving Lorentz violation lead to interesting new effects in short-range experiments that could have escaped detection in conventional studies to date [5]. Couplings of this type emerge naturally as the dominant curvature self interactions in the context of a general treatment of gravity theories using effective field techniques [6], and they imply perturbative corrections to Newton gravity that are inverse quartic and vary with orientation and time. In contrast, the various searches for pure-gravity local Lorentz violation within this framework have been restricted to the context of a Lorentz-violating inverse-square law [7–14].

Here, we present new data from a short-range experiment in Bloomington, IN [15–17], acquired during a run in March 2012. We use these data to perform a search for short-range Lorentz violation involving perturbative inverse-quartic corrections to Newton’s law, thereby obtaining first constraints on quadratic curvature couplings with Lorentz violation at the level of 10^{-9} m^2 . To enable the simultaneous measurement of all independent Lorentz-violating corrections of this type, we also extend the analysis to incorporate the 2002 dataset obtained when the apparatus was located in Boulder, CO [16]. Note that a few other short-range experiments, including those described in Refs. [18–21], may have potential sensitivity

to perturbative effects of this type, while some experiments optimized for nonperturbative corrections to Newton’s law could conceivably be adjusted to study perturbative effects [22–25]. Note also that constraints on forces with various inverse-power laws have appeared in the literature [26], but only in the context of Lorentz-invariant effects.

The design and operation of the experiment is described elsewhere [15–17]. Here, we summarize briefly the basic features. Each of the two test masses is a planar tungsten oscillator of approximate thickness $250\ \mu\text{m}$, separated by a gap of about $80\ \mu\text{m}$. A stiff conducting shield is placed between them to suppress electrostatic and acoustic backgrounds. The planar geometry concentrates as much mass as possible at the scale of interest while being nominally null with respect to inverse-square forces, thereby suppressing the Newton background relative to new short-range effects. The force-sensitive ‘detector’ mass is driven by the force-generating ‘source’ mass at a resonance near 1 kHz. Vibration isolation is a key requirement for this setup, and operation at 1 kHz is chosen because at this frequency a comparatively simple passive vibration-isolation system can be constructed. The entire apparatus is enclosed in a vacuum chamber and operated at 10^{-7} torr to minimize the acoustic coupling. Detector oscillations are read out via a capacitive transducer probe coupled to a sensitive differential amplifier, with the signal fed to a lock-in amplifier referenced by the same waveform used to drive the source mass. This design has proved effective in suppressing all background forces to the extent that only thermal noise is observed, arising from dissipation in the detector mass. The output of the lock-in amplifier constitutes the raw data. These data are converted to force readings by comparison with the detector thermal noise, the scale of which is determined using the equipartition theorem [15]. Following data collection in 2002, this experiment set the strongest limits on unobserved forces of nature between 10 and $100\ \mu\text{m}$ [16]. The apparatus has since been optimized to explore gaps below $50\ \mu\text{m}$, and operation at the thermal noise limit has recently been demonstrated [17].

The solution for the modified Newton force resulting from general Lorentz-violating quartic curvature couplings in the effective field theory approach to gravity [6] involves effective coefficients $(\bar{k}_{\text{eff}})_{jklm}$ for Lorentz violation with dimensions of squared length [5]. Measuring these coefficients is the goal of the present analysis. These 81 coefficients are totally symmetric with indices j, k, l, m ranging over the three spatial directions, so they represent 15 independent observables for Lorentz violation. The coefficients can be taken as constant on the scale of the solar system [27], so following standard convention we extract values of these

coefficients in the canonical Sun-centered frame [3, 28], with Z axis along the direction of the Earth's rotation and X axis pointing towards the vernal equinox. Due to the rotation of the Earth relative to the Sun-centered frame, the coefficients measured in the laboratory vary with sidereal time T . The Earth's boost $\beta_{\oplus} \simeq 10^{-4}$ can be neglected here. The transformation from the Sun-centered frame (X, Y, Z) to the laboratory frame (x, y, z) therefore involves a time-dependent rotation $R^{jJ}(T)$. With the laboratory z axis pointing to the local zenith and the x axis pointing to local south, the rotation matrix is

$$R^{jJ}(T) = \begin{pmatrix} \cos \chi \cos \omega_{\oplus} T & \cos \chi \sin \omega_{\oplus} T & -\sin \chi \\ -\sin \omega_{\oplus} T & \cos \omega_{\oplus} T & 0 \\ \sin \chi \cos \omega_{\oplus} T & \sin \chi \sin \omega_{\oplus} T & \cos \chi \end{pmatrix}, \quad (1)$$

where $\omega_{\oplus} \simeq 2\pi/(23 \text{ h } 56 \text{ min})$ is the Earth's sidereal frequency. The angle χ is the colatitude of the laboratory, which is 0.887 in Bloomington and 0.872 in Boulder. The laboratory coefficients $(\bar{k}_{\text{eff}})_{jklm}(T)$ are thus related to the coefficients $(\bar{k}_{\text{eff}})_{JKLM}$ in the Sun-centered frame by

$$(\bar{k}_{\text{eff}})_{jklm}(T) = R^{jJ} R^{kK} R^{lL} R^{mM} (\bar{k}_{\text{eff}})_{JKLM}. \quad (2)$$

The data analysis requires an explicit expression for the Lorentz violating force arising from the source mass density $\rho(\mathbf{r}')$. The cartesian components $F^j(\mathbf{r}, T)$ of the modified force at position \mathbf{r} and at sidereal time T contain the conventional Newton force along with an inverse-quartic correction term,

$$F^j(\mathbf{r}, T) = -G_N \int d^3 r' \rho(\mathbf{r}') \left(\frac{\hat{R}^j}{|\mathbf{r} - \mathbf{r}'|^2} + \frac{\bar{k}^j(\hat{\mathbf{R}}, T)}{|\mathbf{r} - \mathbf{r}'|^4} \right). \quad (3)$$

Here, $\hat{\mathbf{R}} = (\mathbf{r} - \mathbf{r}')/|\mathbf{r} - \mathbf{r}'|$, while

$$\begin{aligned} \bar{k}^j(\hat{\mathbf{R}}, T) = & \frac{105}{2} (\bar{k}_{\text{eff}})_{klmn} \hat{R}^j \hat{R}^k \hat{R}^l \hat{R}^m \hat{R}^n \\ & - 45 (\bar{k}_{\text{eff}})_{klmm} \hat{R}^j \hat{R}^k \hat{R}^l + \frac{9}{2} (\bar{k}_{\text{eff}})_{klkl} \hat{R}^j \\ & - 30 (\bar{k}_{\text{eff}})_{jklm} \hat{R}^k \hat{R}^l \hat{R}^m + 18 (\bar{k}_{\text{eff}})_{jkl} \hat{R}^k \end{aligned} \quad (4)$$

controls the inverse-quartic force correction, which varies with direction $\hat{\mathbf{R}}$ and sidereal time T . Note that the T dependence is oscillatory and includes components up to the fourth harmonic of ω_{\oplus} .

The detector is a constrained mechanical oscillator with distributed mass. The modal amplitude at any point in the detector mass is strongly dominated by vertical motion. This is particularly true near the thermal noise limit, where the amplitudes are of order 1 pm [17]. The experiment is thus sensitive predominantly to the z component F_p of the effective force at the location of the capacitive probe, which can be written as

$$F_p(T) = \frac{1}{d} \int_D d^3r \xi(\mathbf{r}) F^z(\mathbf{r}, T). \quad (5)$$

Here, $\xi(\mathbf{r})$ is the detector mode-shape function, which is the amplitude of the displacement of the detector at point \mathbf{r} when undergoing free oscillations in the relevant mode of interest, and the displacement d is the oscillation amplitude of the detector at the location of the probe. These quantities are derived from a finite-element model of the detector mass and have the same arbitrary normalization. The integration is taken over the volume D of the detector over which the force is applied.

For the purposes of the present analysis, Eq. (5) is evaluated by Monte-Carlo integration, using the z component $F^z(\mathbf{r})$ of the force (3) expressed in terms of the coefficients $(\bar{k}_{\text{eff}})_{JKLM}$ in the Sun-centered frame along with the geometrical parameters listed in Table II of Ref. [15]. Note that the source amplitude for the 2012 dataset was $22.2 \pm 3.2 \mu\text{m}$ and the average gap was $77.5 \pm 20 \mu\text{m}$. The experiment is performed on resonance, so the Monte-Carlo algorithm computes the Fourier amplitude of Eq. (5) averaged over a complete cycle of the source-mass oscillation, taking into account the measured source-mass curvature and mode shape. The result can be expressed as a Fourier series in the sidereal time T ,

$$F_p(T) = \frac{1}{2}C_0 + \sum_{m=1}^4 S_{m\omega} \sin(m\omega_{\oplus}T) + C_{m\omega} \cos(m\omega_{\oplus}T). \quad (6)$$

The Fourier amplitudes in this expression are functions of the coefficients $(\bar{k}_{\text{eff}})_{JKLM}$, the source and detector mass geometry, and the laboratory colatitude. Using approximately 200 million random pairs of points for each test mass suffices to resolve all harmonics. Systematic errors from the dimensions and positions of the test masses can be determined at this stage, by computing the mean and standard deviation of a population of Fourier amplitudes generated with a spread of geometries based on metrology errors. For the most resolvable terms, the typical systematic error from this source is about 10%. Roughly half the terms have systematic errors exceeding 100%, with geometrical uncertainties swamping the resolution.

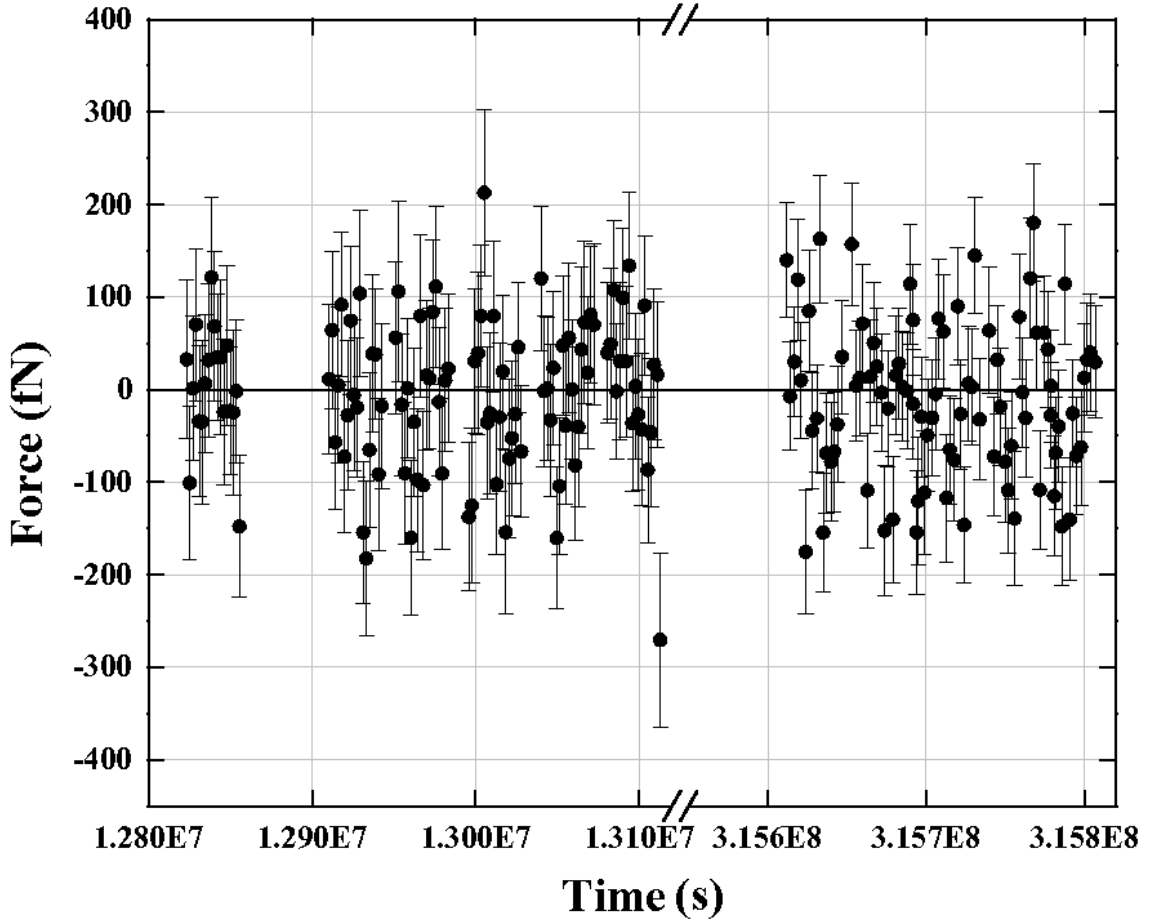


FIG. 1: Data from the Indiana short-range experiment.

In the computation of the amplitudes in the Fourier series (6), all 15 independent components of $(\bar{k}_{\text{eff}})_{JKLM}$ appear. However, the zero in the rotation matrix (1) insures no single amplitude contains all 15 degrees of freedom. The transformation (2) also predicts some simple relations among the amplitudes, each of which is satisfied by the results of the numerical integration. Performing the numerical integration for a hypothetical geometry with an average gap an order of magnitude larger than the largest dimension of either mass produces a result agreeing to within a few percent with the analytical expression for point masses of the same mass and separation. This limiting case reveals some contributions from $(\bar{k}_{\text{eff}})_{JKLM}$ are resolvable only due to the planar geometry.

Time stamps in the data are extracted and offset relative to $T = 0$ in the Sun-centered frame, taken to be the 2002 vernal equinox. Figure 1 displays force data as a function of sidereal time T , including data acquired during the runs in 2012 and in 2002. The force data were collected at a 1 Hz rate in 14.4-minute sets (2012 run) and in 12-minute sets (2002

run), with comparable intervals between each set during which diagnostic data were taken to monitor the experiment for gain and frequency drifts. Each data point represents the mean of a 14.4- or 12-minute set. Each error bar shown is the 1σ standard deviation of the mean, including both the statistical uncertainty and the systematic errors associated with the force calibration listed in Table 1 of Ref. [15]. For the 2012 experiment, the thermal noise voltage was 7.43 ± 0.05 V, the mechanical quality factor was 22479 ± 64 , and the integrated mode shape was $(6.0\pm 0.6)\times 10^{-11}$ m^{5/2}.

Figure 1 represents a finite time series of force data with uneven time distribution. To analyze the data for Lorentz violation, we adopt a well-established procedure [9]. The ideal measure of each harmonic signal component is the corresponding Fourier amplitude in Eq. (6). Each of these nine amplitudes, $k = 1, \dots, 9$, can be estimated by the discrete Fourier transform

$$\tilde{d}_k = \frac{2}{N} \sum_j f(T_j) a_k(T_j), \quad (7)$$

where N is the total number of force-data points plotted in Fig. 1, $f(T_j)$ are the values of the force at each time T_j , and $a_k(T_j)$ is either $\sin(\omega_k T_j)$ or $\cos(\omega_k T_j)$ with $\omega_k = m\omega_\oplus$, $m = 0, 1, 2, 3, 4$. For this part of the analysis, we treat the 2012 and 2002 results as separate datasets. The nine components \tilde{d}_k extracted from the 2012 dataset and from the 2002 dataset are listed in the second and fourth columns of Table I. The uncertainties are determined by propagating the errors of the time-series data in Fig. 1. The uncertainties can also be estimated by computing the Fourier transforms at several frequencies above and below the signal frequency and calculating the root mean square of the values obtained. The former method is slightly more pessimistic and is adopted here.

For a finite time series, the Fourier components overlap. The overlap can be quantified by a correlation covariance matrix $\text{cov}(a_k, a_{k'}) = (2/N) \sum_j a_k(T_j) a_{k'}(T_j)$. The covariance matrix relates the amplitudes \tilde{D}_k for continuous data to the amplitudes \tilde{d}_k for discrete data according to

$$\tilde{d}_k = \sum_{k'} \text{cov}(a_k, a_{k'}) \tilde{D}_{k'}. \quad (8)$$

The nine continuous amplitudes \tilde{D}_k can be obtained by applying the inverse matrix cov^{-1} to Eq. (8). For the 2012 and 2002 datasets, the results of this calculation are also displayed in the third and fifth columns of Table I. The \tilde{D}_k can be taken to represent the measured values of the force components.

	2012 data	2012 data	2002 data	2002 data
Mode	\tilde{d}_k	\tilde{D}_k	\tilde{d}_k	\tilde{D}_k
c_0	-8.1 ± 5.0	-3.1 ± 6.2	-4.2 ± 7.8	1.7 ± 19.2
s_ω	-0.1 ± 6.9	2.1 ± 8.5	-24.5 ± 9.6	-14.0 ± 22.9
c_ω	-7.5 ± 7.3	-7.5 ± 8.0	5.0 ± 12.2	4.2 ± 11.5
$s_{2\omega}$	-6.1 ± 7.1	-12.4 ± 8.9	-16.7 ± 12.0	-6.7 ± 12.6
$c_{2\omega}$	-8.3 ± 7.0	-8.8 ± 7.4	3.1 ± 9.9	-9.7 ± 26.4
$s_{3\omega}$	20.2 ± 7.1	23.0 ± 7.9	-25.2 ± 10.4	-23.2 ± 20.7
$c_{3\omega}$	5.4 ± 7.1	8.4 ± 8.6	29.3 ± 11.5	26.8 ± 12.8
$s_{4\omega}$	0.7 ± 7.1	-0.3 ± 7.2	4.5 ± 11.2	9.9 ± 14.1
$c_{4\omega}$	3.5 ± 7.0	-1.0 ± 8.5	7.9 ± 10.8	5.0 ± 21.6

TABLE I: Fourier transforms in fN units.

Individual measurements of the independent components of $(\bar{k}_{\text{eff}})_{JKLM}$ can be extracted from a global probability distribution formed using the values of the nine continuous amplitudes \tilde{D}_k and their errors. Each measured amplitude can be assigned a corresponding probability distribution $p_k = p_k((\bar{k}_{\text{eff}})_{JKLM})$ that is a function of the 15 independent components of $(\bar{k}_{\text{eff}})_{JKLM}$. The p_k are assumed to be Gaussian with means μ_k and standard deviations σ_k . The global probability distribution $P_k = P_k((\bar{k}_{\text{eff}})_{JKLM})$ of interest is then the product of the individual p_k , taking the form

$$P_k = P_0 \exp \left[- \sum_{k=1}^9 \frac{(\tilde{D}_k - \mu_k)^2}{2\sigma_k^2} \right]. \quad (9)$$

In this expression, P_0 is an arbitrary normalization. The predicted signal $\mu_k = \mu_k((\bar{k}_{\text{eff}})_{JKLM})$ for the k th amplitude is determined from Eqs. (5) and (6), and the variance σ_k^2 includes all statistical and systematic errors.

An independent measurement of any one chosen component of $(\bar{k}_{\text{eff}})_{JKLM}$ can in principle be obtained by integrating the global probability distribution P_k over all other components. The result of this procedure is a distribution involving the chosen component with a single mean and standard deviation, which constitute the estimated component measurement and its error. However, the 2012 dataset alone contains only nine signal components, which is insufficient to constrain independently each of the 15 degrees of freedom in $(\bar{k}_{\text{eff}})_{JKLM}$.

Coefficient	2012 value (10^{-9} m ²)	2002 value (10^{-9} m ²)	Combined (10^{-9} m ²)
$(\bar{k}_{\text{eff}})_{XXXX}$	0.5 ± 1.2	0.2 ± 8.1	0.5 ± 1.1
$(\bar{k}_{\text{eff}})_{YYYY}$	-0.1 ± 1.1	-0.9 ± 8.1	-0.1 ± 1.0
$(\bar{k}_{\text{eff}})_{ZZZZ}$	0.3 ± 3.9	-0.3 ± 7.1	0.2 ± 1.2
$(\bar{k}_{\text{eff}})_{XXXY}$	1.2 ± 4.4	1.2 ± 5.2	1.0 ± 1.7
$(\bar{k}_{\text{eff}})_{XXZX}$	0.5 ± 4.5	-0.5 ± 2.9	0.3 ± 0.8
$(\bar{k}_{\text{eff}})_{YYYX}$	1.2 ± 4.4	1.3 ± 5.2	1.0 ± 1.7
$(\bar{k}_{\text{eff}})_{YYYZ}$	-0.1 ± 2.6	1.8 ± 5.8	-0.1 ± 0.9
$(\bar{k}_{\text{eff}})_{ZZZX}$	0.5 ± 4.5	-0.5 ± 2.9	0.3 ± 0.8
$(\bar{k}_{\text{eff}})_{ZZZY}$	-1.6 ± 4.4	1.8 ± 5.7	-0.1 ± 1.1
$(\bar{k}_{\text{eff}})_{XXYY}$	0.2 ± 5.2	-0.2 ± 4.4	0.1 ± 0.8
$(\bar{k}_{\text{eff}})_{XXZZ}$	0.2 ± 0.8	0.0 ± 3.9	0.2 ± 0.6
$(\bar{k}_{\text{eff}})_{YYZZ}$	0.0 ± 0.8	-0.3 ± 3.9	0.0 ± 0.6
$(\bar{k}_{\text{eff}})_{XXYZ}$	-0.2 ± 4.6	1.8 ± 5.8	-0.1 ± 1.1
$(\bar{k}_{\text{eff}})_{YYXZ}$	0.5 ± 4.6	-0.5 ± 2.9	0.3 ± 0.8
$(\bar{k}_{\text{eff}})_{ZZXY}$	1.2 ± 4.6	1.3 ± 5.2	1.0 ± 1.7

TABLE II: Coefficient values (2σ) from the 2012, 2002, and combined datasets, with all other coefficients vanishing.

Following standard practice in the field [3], we can obtain maximum-sensitivity constraints on each component of $(\bar{k}_{\text{eff}})_{JKLM}$ in turn by integrating the global probability distribution with the other 14 degrees of freedom set to zero. The resulting measurements and 2σ errors on each independent component of $(\bar{k}_{\text{eff}})_{JKLM}$ are displayed in the first two columns of Table II. Note that the first column reveals our choice for the 15 independent components of $(\bar{k}_{\text{eff}})_{JKLM}$, in terms of which all 81 components can be obtained using symmetry. Note also that the sensitivity of the apparatus to the coefficients $(\bar{k}_{\text{eff}})_{JKLM}$ can be crudely estimated as the ratio of the thermal-noise force at the location of the probe (~ 10 fN) to the scale ($\sim 10 \mu\text{N}/\text{m}^2$) of the amplitudes in the Fourier series (6), in agreement with the size of the values in the second column of Table II.

The third column of Table II displays the values for the coefficients $(\bar{k}_{\text{eff}})_{JKLM}$ obtained

Coefficient	Value (m ²)
$(\bar{k}_{\text{eff}})_{XXXX}$	$(-0.1 \pm 1.8) \times 10^{-2}$
$(\bar{k}_{\text{eff}})_{YYYY}$	$(-0.1 \pm 1.8) \times 10^{-2}$
$(\bar{k}_{\text{eff}})_{ZZZZ}$	$(-0.1 \pm 3.3) \times 10^{-2}$
$(\bar{k}_{\text{eff}})_{XXXY}$	$(0.1 \pm 2.1) \times 10^{-6}$
$(\bar{k}_{\text{eff}})_{XXZX}$	$(-0.6 \pm 2.9) \times 10^{-6}$
$(\bar{k}_{\text{eff}})_{YYYX}$	$(0.3 \pm 1.8) \times 10^{-6}$
$(\bar{k}_{\text{eff}})_{YYYZ}$	$(0.0 \pm 1.5) \times 10^{-6}$
$(\bar{k}_{\text{eff}})_{ZZZX}$	$(0.4 \pm 1.2) \times 10^{-6}$
$(\bar{k}_{\text{eff}})_{ZZZY}$	$(-0.3 \pm 2.2) \times 10^{-6}$
$(\bar{k}_{\text{eff}})_{XXYY}$	$(-0.2 \pm 9.4) \times 10^{-3}$
$(\bar{k}_{\text{eff}})_{XXZZ}$	$(0.1 \pm 1.8) \times 10^{-2}$
$(\bar{k}_{\text{eff}})_{YYZZ}$	$(0.1 \pm 1.8) \times 10^{-2}$
$(\bar{k}_{\text{eff}})_{XXYZ}$	$(3.0 \pm 8.4) \times 10^{-7}$
$(\bar{k}_{\text{eff}})_{YYXZ}$	$(2.1 \pm 9.4) \times 10^{-7}$
$(\bar{k}_{\text{eff}})_{ZZXY}$	$(-0.1 \pm 1.7) \times 10^{-6}$

TABLE III: Coefficient values (2σ) from the combined datasets, with all coefficients contributing simultaneously.

from a comparable analysis of the 2002 dataset. These 2002 results are about a factor of five less sensitive than the 2012 data, a feature that can be traced to the larger average gap between the source and detector masses and the smaller source-mass amplitude in the 2002 experiment. The final column of Table II presents the measured values of each independent component taken in turn that are obtained from analyzing the combined datasets.

Although the 2002 results are less sensitive to Lorentz violation, the nine associated signal components contain different linear combinations of the 15 degrees of freedom in the coefficients $(\bar{k}_{\text{eff}})_{JKLM}$. Performing a simultaneous analysis of the 2012 and the 2002 datasets therefore permits measurements of every independent degree of freedom in $(\bar{k}_{\text{eff}})_{JKLM}$ when all 15 contribute simultaneously. The range of k in Eqs. (7)-(9) then includes 18 values, but the structure of the calculations is otherwise as described above. The results from this joint-dataset analysis are presented in Table III.

The contents of Tables II and III represent the first measurements of possible short-range Lorentz violation involving perturbative inverse-quartic corrections to Newton’s law and hence of possible quadratic curvature couplings violating local Lorentz invariance. Upgrading the apparatus by improving the test-mass and shield flatness could reduce the average gap by a factor of two, and refining the test-mass metrology could reduce the uncertainty in the average gap by a factor of four. Simulations suggest these improvements would increase the overall sensitivity by more than an order of magnitude in the absence of new systematics. Moreover, with several months of run time, the statistical error bars could be reduced by about another order of magnitude. The prospects are excellent for further sharpening short-range tests of Lorentz symmetry in gravity.

We thank Q. Bailey, R. Decca, and R. Xu for discussions, S. Kelly for collection of the 2012 data, and D. Bennett and W. Jensen for work on the Monte-Carlo code in earlier incarnations of this experiment. The 2012 data were taken at the Indiana University Center for the Exploration of Energy and Matter. This work was supported in part by the National Science Foundation under grant number PHY-1207656, by the Department of Energy under grant number DE-FG02-13ER42002, and by the Indiana University Center for Spacetime Symmetries.



- [1] V.A. Kostelecký and S. Samuel, *Phys. Rev. D* **39**, 683 (1989); V.A. Kostelecký and R. Potting, *Nucl. Phys. B* **359**, 545 (1991); *Phys. Rev. D* **51**, 3923 (1995).
- [2] For reviews see, for example, J. Murata and S. Tanaka, arXiv:1408.3588; J. Jaeckel and A. Ringwald, *Ann. Rev. Nucl. Part. Sci.* **60**, 405 (2010); E.G. Adelberger, J.H. Gundlach, B.R. Heckel, S. Hoedl, and S. Schlamminger, *Prog. Part. Nucl. Phys.* **62**, 102 (2009); E. Fischbach and C. Talmadge, *The Search for Non-Newtonian Gravity*, Springer-Verlag, 1999.
- [3] V.A. Kostelecký and N. Russell, *Data Tables for Lorentz and CPT Violation*, 2014 edition, arXiv:0801.0287v7.
- [4] C.M. Will, *Liv. Rev. Rel.* **17**, 4 (2014).
- [5] Q.G. Bailey, V.A. Kostelecký, and R. Xu, arXiv:1410.6162.
- [6] V.A. Kostelecký, *Phys. Rev. D* **69**, 105009 (2004).
- [7] J.B.R. Battat, J.F. Chandler, and C.W. Stubbs, *Phys. Rev. Lett.* **99**, 241103 (2007).

- [8] H. Müller, S.-w. Chiow, S. Herrmann, S. Chu, and K.-Y. Chung, *Phys. Rev. Lett.* **100**, 031101 (2008).
- [9] K.-Y. Chung, S.-w. Chiow, S. Herrmann, S. Chu, and H. Müller, *Phys. Rev. D* **80**, 016002 (2009).
- [10] D. Bennett, V. Skavysh, and J. Long, in V.A. Kostelecký, ed., *CPT and Lorentz Symmetry V*, World Scientific, Singapore 2011.
- [11] L. Iorio, *Class. Quant. Grav.* **29**, 175007 (2012).
- [12] Q.G. Bailey, R.D. Everett, and J.M. Overduin, *Phys. Rev. D* **88**, 102001 (2013).
- [13] L. Shao, *Phys. Rev. Lett.* **112**, 111103 (2014); arXiv:1412.2320.
- [14] Q.G. Bailey and V.A. Kostelecký, *Phys. Rev. D* **74**, 045001 (2006).
- [15] J.C. Long, H.W. Chan, A.B. Churnside, E.A. Gulbis, M.C.M. Varney, and J.C. Price, arXiv:hep-ph/0210004.
- [16] J.C. Long, H.W. Chan, A.B. Churnside, E.A. Gulbis, M.C.M. Varney, and J.C. Price, *Nature* **421**, 922 (2003).
- [17] H. Yan, E.A. Housworth, H.O. Meyer, G. Visser, E. Weisman, and J.C. Long, *Class. Quant. Grav.* **31**, 205007 (2014).
- [18] C.D. Hoyle, D.J. Kapner, B.R. Heckel, E.G. Adelberger, J.H. Gundlach, U. Schmidt, and H.E. Swanson, *Phys. Rev. D* **70**, 042004 (2004); D.J. Kapner, T.S. Cook, E.G. Adelberger, J.H. Gundlach, B.R. Heckel, C.D. Hoyle, and H.E. Swanson, *Phys. Rev. Lett.* **98**, 021101 (2007).
- [19] L.C. Tu, S.-G. Guan, J. Luo, C.-G. Shao, and L.-X. Liu, *Phys. Rev. Lett.* **98**, 201101 (2007); S.-Q. Yang, B.-F. Zhan, Q.-L. Wang, C.-G. Shao, L.C. Tu, W.-H. Tan, and J. Luo, *Phys. Rev. Lett.* **108**, 081101 (2012).
- [20] J. Murata *et al.*, *High Energy News* **32**, 233 (2014).
- [21] J.K. Hoskins, R.D. Newman, R. Spero, and J. Schultz, *Phys. Rev. D* **32**, 3084 (1985).
- [22] R.S. Decca, D. Lopez, H.B. Chan, E. Fischbach, D.E. Krause and C.R. Jamell, *Phys. Rev. Lett.* **94**, 240401 (2005); Y.-J. Chen, W.K. Tham, D.E. Krause, D. Lopez, E. Fischbach, and R.S. Decca arXiv:1410.7267.
- [23] J. Chiaverini, S.J. Smullin, A.A. Geraci, D.M. Weld, and A. Kapitulnik, *Phys. Rev. Lett.* **90**, 151101 (2003); S.J. Smullin, A.A. Geraci, D.M. Weld, J. Chiaverini, S.P. Holmes, and A. Kapitulnik, *Phys. Rev. D* **72**, 122001 (2005); A.A. Geraci, S.J. Smullin, D.M. Weld, J. Chiaverini, and A. Kapitulnik, *Phys. Rev. D* **78**, 022002 (2008).

- [24] A.A. Geraci, S.B. Papp, and J. Kitching, Phys. Rev. Lett. **105**, 101101 (2010).
- [25] F. Sorrentino, Q. Bodart, L. Cacciapuoti, Y.-H. Lien, M. Prevedelli, G. Rosi, L. Salvi, and G.M. Tino, Phys. Rev. A **89**, 2 (2014).
- [26] E.G. Adelberger, B.R. Heckel, S.A. Hoedl, C.D. Hoyle, D.J. Kapner, and A. Upadhye, Phys. Rev. Lett. **98**, 131104 (2007).
- [27] D. Colladay and V.A. Kostelecký, Phys. Rev. D **55**, 6760 (1997); Phys. Rev. D **58**, 116002 (1998).
- [28] R. Bluhm *et al.*, Phys. Rev. D **68**, 125008 (2003); Phys. Rev. Lett. **88**, 090801 (2002); V.A. Kostelecký and M. Mewes, Phys. Rev. D **66**, 056005 (2002).